

Radiative Capture $d(\alpha, \gamma)^6\text{Li}$ Reaction in Cluster Effective Field Theory

F. Nazari^{*} and M. Radin[†]

Department of Physics, K. N. Toosi University of Technology, P.O.Box 16315-1618, Tehran, Iran

M. Moeini Arani[‡]

Malek Ashtar University of Technology, Tehran, Iran

In this study, we focus on the radiative capture process of the deuteron on alpha particle leading to the formation of ^6Li in the two-body formalism through the cluster effective field theory(EFT). This was the primitive nuclear reaction producing ^6Li a few minutes after the Big Bang. In detail, we outline the calculation of the dominant $E1$ and $E2$ electromagnetic transition amplitudes of $d(\alpha, \gamma)^6\text{Li}$ up to next-to-leading order. Then we obtain the astrophysical S-factor by fitting it to the experimental data. Finally, we compare the obtained EFT results for the astrophysical S-factor with the other theoretical results.

Keywords. Cluster Effective Field Theory, Gamma Capture Reaction, Electromagnetic Transition, Astrophysical S-factor.

PACS. 21.45-v Few-body systems - 11.10.-z Field theory - 03.65.Nk Scattering theory

I. INTRODUCTION

In the standard Big Bang Nucleosynthesis (BBN) framework, the primitive ^6Li abundance is mainly determined by two nuclear reactions: the $d(\alpha, \gamma)^6\text{Li}$ reaction, where deuteron reacts with an alpha particle to produce ^6Li . This reaction leads to the formation of ^6Li during the primordial nucleosynthesis process [1, 2]. Conversely, $^6\text{Li}(p, \alpha)^3\text{He}$ can destroy ^6Li . In this reaction, ^6Li reacts with a proton to produce an alpha particle and ^3He . This

^{*}Electronic address: f.nazari@email.kntu.ac.ir

[†]Electronic address: radin@kntu.ac.ir

[‡]Electronic address: m.moeini.a@ut.ac.ir

reaction reduces the abundance of ${}^6\text{Li}$ in the early universe. This reaction rate is commonly understood within the BBN energy range and has been extensively researched using various techniques[3–7].

Consequently, the ${}^6\text{Li}$ production reaction has recently been a prime focus of studies, both experimentally and theoretically [8–17]. The available experimental data for this reaction cover the region $100\text{keV} \leq E_{CM} \leq 4\text{MeV}$ [1, 18–22]. The low-energy experimental data have been obtained indirectly from measurements using the Coulomb breakup process ${}^6\text{Li} + {}^{208}\text{Pb} \rightarrow \alpha + d + {}^{208}\text{Pb}$ [21]. The most historical theoretical calculations of the low-energy cross section for the reaction has been performed within the framework of the microscopic resonating group method, in the quasi-microscopic potential model and the framework of the multicluster dynamic model [23–25].

In the present work, we focus on applying cluster effective field theory (CEFT) formalism as one of the most precise techniques for low-energy nuclear processes for the investigation of gamma capture $d(\alpha, \gamma){}^6\text{Li}$ reaction. The CEFT is the ideal tool to analyze the features of halo states with minimal assumptions [26, 27]. It describes systems using their effective degrees of freedom, i.e., core and valence nucleons, and interactions that are dictated by low-energy constants. CEFT was formulated in the study of the shallow p-wave neutron-alpha resonance and applied to other systems, such as the s-wave alpha-alpha resonance, electromagnetic transitions, and capture reactions. In this paper, we apply this idea to the $d(\alpha, \gamma){}^6\text{Li}$ radiative reaction, following a cluster approach of point-like objects. Our investigation leads to calculating the astrophysical S-factor of the mentioned reaction.

The manuscript is organized as follows: In Sec. II, the possible and dominant electromagnetic transition of the $d(\alpha, \gamma){}^6\text{Li}$ reaction was introduced. Moreover, The effective non-relativistic lagrangian of the system was presented, concluding the scattering and additional terms for the radiative capture process. The details of the Coulomb interaction were investigated in this section. Sec. III is dedicated to the basic feature of the elastic scattering $d(\alpha, \alpha)d$ reaction in CEFT. In Sec. IV, we review the principles of radiative capture reaction. Furthermore, we derive relevant expressions for the capture amplitude and cross-section for the $E1$ and $E2$ transitions in this section. Sec. V collects the numerical results, in particular, the astrophysical S-factor at leading and next-to-leading order. Our concluding remarks are presented in Sec. VI.

II. RADIATIVE CAPTURE REACTION

In this section, we first discuss the possible and most prevalent electromagnetic transitions that occur during the radiative capture process of $d(\alpha, \gamma)^6\text{Li}$ at low energies. Then, we present the Lagrangian of this reaction based on two-body CEFT. From a schematic point of view, in a radiative capture reaction, a stationary nucleus in a definite quantum mechanical state transitions to a lower energy state via the emission of a single photon. The conservation of angular momentum plays a controlling role in the gamma ray decay process. Both the initial and final states of the nucleus will possess a precise angular momentum and parity, necessitating the photon to connect these two states while preserving both parity and angular momentum. Photons carry a precise amount of angular momentum and possess a specific parity, with the conservation of these properties influencing the characteristics of the emitted photon. The electromagnetic selection rules and multipolarities for nuclear physics are outlined in Table. I.

TABLE I: The electromagnetic selection rules. Δl and $\Delta\pi$ are angular momentum and parity of the photon.

Radiation Type	Name	Δl	$\Delta\pi$
$E1$	Electric dipole	1	yes
$M1$	Magnetic dipole	1	no
$E2$	Electric quadrupole	2	no
$M2$	Magnetic quadrupole	2	yes

Generally, the type of photon involved in a transition between nuclei can be determined by considering the properties of photons. First, the parity of the photon ($\Delta\pi$) is determined by the difference in parities of the two nuclear states. The photon angular momentum is then constrained within the range of $|l_i - l_f| \leq \Delta l \leq l_i + l_f$, where l_i and l_f are the angular momenta of the initial and final states of the nucleus, respectively. The multipolarity of the photon is specified by the amount of angular momentum carried by the photon [28].

Considering the alpha (spin-zero) and deuteron (spin-one) particles as point-like particles and taking into account the l -wave components of the two-body $d - \alpha$ system, the possible

incoming states for the two-body $d - \alpha$ system are $\xi = {}^3S_1, {}^3P_0, {}^3P_1, {}^3P_2, {}^3D_1, {}^3D_2, {}^3D_3$ corresponding to the relevant spin-angular momenta, $j = 0, 1, 2, 3$. Considering the alpha (spin-zero) and deuteron (spin-one) particles as point-like particles and taking into account the l -wave components of the two-body $d - \alpha$ system, the possible incoming states for the two-body $d - \alpha$ system are $\xi = {}^3S_1, {}^3P_0, {}^3P_1, {}^3P_2, {}^3D_1, {}^3D_2, {}^3D_3$ corresponding to the relevant spin-angular momenta, $j = 0, 1, 2, 3$. Thus, we consider the final ground state of the ${}^6\text{Li}$ nucleus with $J^\pi = 1^+$ as 3S_1 . According to the electromagnetic transition rules of nuclear physics, the $E1$ and $E2$ transitions contribute to the $d(\alpha, \gamma){}^6\text{Li}$ radiative capture amplitude in the low-energy regime. Transitions from P -waves to S -wave, which change parity and result in an angular momentum change of $\Delta l = 1$, are considered $E1$ transitions. Transitions from D -waves to S -wave, which does not change parity but involves an angular momentum change of $\Delta l = 2$, contribute to the $E2$ transition. Therefore, the possible electromagnetic transitions during the radiative capture process in the $d(\alpha, \gamma){}^6\text{Li}$ reaction at low energies can be outlined as follows

$${}^3P_0, {}^3P_1, {}^3P_2 \xrightarrow{E1} {}^3S_1, \quad {}^3D_1, {}^3D_2, {}^3D_3 \xrightarrow{E2} {}^3S_1.$$

A. Effective Lagrangian

In this study, we consider the deuteron and alpha as point-like particles. Therefore, in the cluster EFT that we construct for the $d - \alpha$ system, the degrees of freedom are only the alpha and deuteron particles, and the ${}^6\text{Li}$ nucleus treats as a bound state of point-like nuclear clusters alpha and deuteron with a binding energy $B = 1.47 \text{ MeV}$. Therefore, the effective non-relativistic Lagrangian which describes the dynamics in all possible channels ξ , can be written as

$$\mathcal{L}^{[\xi]} = \mathcal{L}_{ES}^{[\xi]} + \mathcal{L}_{RC}^{[\xi]}, \quad (1)$$

where $\mathcal{L}_{ES}^{[\xi]}$ defines the elastic scattering and $\mathcal{L}_{RC}^{[\xi]}$ denotes the additional terms for the radiative capture process. The Lagrangian $\mathcal{L}_{ES}^{[\xi]}$ is given by [29]

$$\begin{aligned} \mathcal{L}_{ES}^{[\xi]} = & \phi^\dagger \left(i\partial_0 + \frac{\nabla^2}{2m_\alpha} \right) \phi + d_i^\dagger \left(i\partial_0 + \frac{\nabla^2}{2m_d} \right) d_i + \eta^{[\xi]} t^{[\xi]\dagger} \left[i\partial_0 + \frac{\nabla^2}{2m_t} - \Delta^{[\xi]} \right] t^{[\xi]} \\ & + g^{[\xi]} [t^{[\xi]\dagger} (\phi \Pi^{[\xi]} d) + h.c.] + h^{[\xi]} t^{[\xi]\dagger} \left[\left(i\partial_0 + \frac{\nabla^2}{2m_t} \right)^2 \right] t^{[\xi]} + \dots, \end{aligned} \quad (2)$$

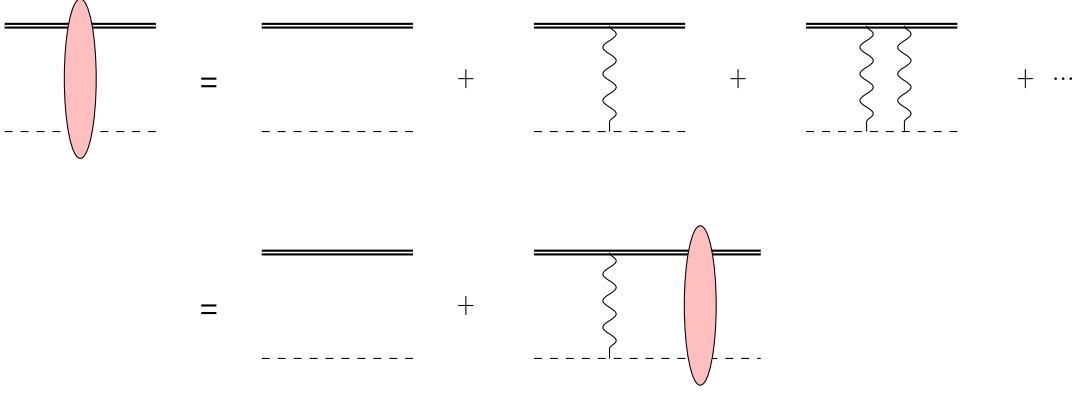


FIG. 1: Coulomb ladder diagrams. The single dashed and double lines represent the scalar α and vector deuteron particle, respectively. The wavy lines represent the exchanged photons.

where "...” stands for the terms with more derivatives and/or auxiliary fields. The scalar field ϕ represents the spinless α field with a mass of $m_\alpha = 3727.38$ MeV, and the vector field $d_i = \varepsilon_i^d d$ indicates the deuteron nucleus auxiliary field with a mass of $m_d = 1875.61$ MeV. The sign $\eta^{[\xi]}$ is used to match the sign of the effective range $r^{[\xi]}$ and reflects the auxiliary character of the dimeron field. The coupling constants $\Delta^{[\xi]}$, $g^{[\xi]}$ and $h^{[\xi]}$ for each channel cannot be measured directly, but their renormalized values are determined by matching to the available experimental data of phase shifts as we did in the previous work [29]. The dimeron field $t^{[\xi]}$ with a mass of $m_t = m_d + m_\alpha$, and projection operator $\Pi^{[\xi]}$ for each channel ξ are defined as

$$t^{[\xi]} = \left\{ \begin{array}{ll} \bar{t}_i, & \xi = {}^3S_1 \\ t, & \xi = {}^3P_0 \\ t_k, & \xi = {}^3P_1 \\ t_{ij}, & \xi = {}^3P_2 \\ \tilde{t}_j, & \xi = {}^3D_1 \\ \tilde{t}_{kl}, & \xi = {}^3D_2 \\ \tilde{t}_{kji}, & \xi = {}^3D_3 \end{array} \right\}, \quad \Pi^{[\xi]} = \left\{ \begin{array}{ll} \varepsilon_i^d, & \xi = {}^3S_1 \\ \sqrt{3} \mathcal{P}_i \varepsilon_i^d, & \xi = {}^3P_0 \\ \sqrt{3/2} \epsilon_{kji} \mathcal{P}_j \varepsilon_i^d, & \xi = {}^3P_1 \\ 3/\sqrt{5} \mathcal{P}_j \varepsilon_i^d, & \xi = {}^3P_2 \\ 3/\sqrt{2} \tau_{ji} \varepsilon_i^d, & \xi = {}^3D_1 \\ \sqrt{3/2} \epsilon_{ijl} \tau_{kj} \varepsilon_i^d, & \xi = {}^3D_2 \\ \sqrt{45/8} \tau_{kj} \varepsilon_i^d, & \xi = {}^3D_3 \end{array} \right\}, \quad (3)$$

with the derivative operators, which are introduced as

$$\mathcal{P}_i = \frac{\mu}{i} \left(\frac{\vec{\nabla}_i}{m_d} - \frac{\overleftarrow{\nabla}_i}{m_\alpha} \right), \quad \tau_{ij} = \mathcal{P}_i \mathcal{P}_j - \frac{1}{3} \delta_{ij} \mathcal{P}_k \mathcal{P}_k. \quad (4)$$

The one-body currents are considered by coupling the external photon through minimal substitution, $\nabla \rightarrow \nabla + ieZ\mathbf{A}$ in the Lagrangian $\mathcal{L}_{ES}^{[\xi]}$, where Z is the charge number and \mathbf{A}

is the photon field. The $E1$ two-body currents using the auxiliary fields and corresponding projection operators of Eq. 3 for incoming 3P_0 , 3P_1 and 3P_2 channels can be described as [30]

$$\mathcal{L}_{RC}^{[{}^3P_0]} = -\sqrt{3} \mu Q_1 L_{E1} g^{[{}^3P_0]} g^{[{}^3S_1]} t \bar{t}_i \partial_0 A_i, \quad (5)$$

$$\mathcal{L}_{RC}^{[{}^3P_1]} = -\sqrt{3/2} \mu Q_1 L_{E1} g^{[{}^3P_1]} g^{[{}^3S_1]} \epsilon_{kij} t_k \bar{t}_i \partial_0 A_j, \quad (6)$$

$$\mathcal{L}_{RC}^{[{}^3P_2]} = -3/\sqrt{5} \mu Q_1 L_{E1} g^{[{}^3P_2]} g^{[{}^3S_1]} t_{ij} \bar{t}_i \partial_0 A_j, \quad (7)$$

where μ is the reduced mass of the $d - \alpha$ system. Moreover, the $E2$ two-body currents for incoming 3D_1 , 3D_2 and 3D_3 channels are included by the following Lagrangian [31]

$$\mathcal{L}_{RC}^{[{}^3D_1]} = 3/\sqrt{2} \mu Q_2 L_{E2} g^{[{}^3D_1]} g^{[{}^3S_1]} \tilde{t}_j \bar{t}_i \left(\nabla_j \nabla_i A_0 - \partial_0 (\nabla_j A_i + \nabla_i A_j) / 2 \right), \quad (8)$$

$$\mathcal{L}_{RC}^{[{}^3D_2]} = \sqrt{3/2} \mu Q_2 L_{E2} g^{[{}^3D_2]} g^{[{}^3S_1]} \epsilon_{ijl} \tilde{t}_{kl} \bar{t}_i \left(\nabla_k \nabla_j A_0 - \partial_0 (\nabla_k A_j + \nabla_j A_k) / 2 \right), \quad (9)$$

$$\mathcal{L}_{RC}^{[{}^3D_3]} = \sqrt{45/8} \mu Q_2 L_{E2} g^{[{}^3D_3]} g^{[{}^3S_1]} \tilde{t}_{kji} \bar{t}_i \left(\nabla_k \nabla_j A_0 - \partial_0 (\nabla_k A_j + \nabla_j A_k) / 2 \right). \quad (10)$$

The effective charges $Q_1 = e\mu(Z_d/m_d - Z_\alpha/m_\alpha)$, $Q_2 = e\mu^2(Z_\alpha/m_\alpha^2 + Z_d/m_d^2)$, and $g^{[{}^3S_1]}$, $g^{[\xi]}$ factors are included in the definition of the couplings L_{E1} and L_{E2} . Here, $Z_\alpha=2$ and $Z_d=1$ represent the atomic numbers of the alpha particle and deuteron, respectively.

B. Coulomb interaction

The strength of the Coulomb-photon exchanges in the $d - \alpha$ interaction is quantified by the dimensionless Sommerfeld parameter $\eta_p = k_C/p = Z_\alpha Z_d \alpha_{em} \mu/p$, where k_C is the inverse of the Bohr radius of the $d - \alpha$ system, $\alpha_{em} = e^2/4\pi \sim 1/137$ represents the fine structure constant, and p is the relative momentum of the alpha and deuteron in the center-of-mass (CM) framework. Since, each photon-exchange insertion is proportional to η_p so, in the low-energy scattering region, where the momentum, p , is much less than the characteristic momentum scale k_C , it is important to take into account the full Coulomb interaction in a non-perturbative manner, as illustrated in Fig. 1.

To consider the contribution of the Coulomb interaction in the two-body $d - \alpha$ system, we use the Coulomb Green's function as follows [32]. As depicted in Fig. 1, the Coulomb Green's function is linked to the free Green's function through the integral equation $\hat{G}_C^\pm = \hat{G}_0^\pm + \hat{G}_0^\pm \hat{V}_C \hat{G}_C^\pm$, where $\hat{G}_0^\pm = 1/(E - \hat{H}_0 \pm i\epsilon)$ and $\hat{G}_C^\pm = 1/(E - \hat{H}_0 - \hat{V}_C \pm i\epsilon)$ are the free and Coulomb Green's functions for the $d - \alpha$ system with $\hat{V}_C = 2\alpha_{em}/r$ and $\hat{H}_0 = \hat{p}^2/2\mu$ as the repulsive Coulomb potential between alpha and deuteron and the free-particle Hamiltonian,

respectively. The signs (\pm) correspond to the retarded and advanced Green's functions. The Coulomb wave functions and the retarded Green's function can be obtained by solving the Schrodinger equation with the full Hamiltonian $\hat{H} = \hat{H}_0 + \hat{V}_C$ as [33, 34]

$$\chi_p^{(+)}(\mathbf{r}) = \sum_{l=0}^{\infty} (2l+1) P_l(\hat{\mathbf{p}} \cdot \hat{\mathbf{r}}) \chi_p^{(l)}(r), \quad (11)$$

$$\chi_p^{(l)}(r) = i^l e^{i\sigma_l} \frac{F_l(\eta_p, pr)}{pr}, \quad (12)$$

$$G_C^{(+)}(E, \mathbf{r}', \mathbf{r}) = \sum_{l=0}^{\infty} (2l+1) P_l(\hat{\mathbf{r}}' \cdot \hat{\mathbf{r}}) G_C^{(l)}(E, r', r), \quad (13)$$

$$G_C^{(l)}(E, r', r) = -\frac{\mu p}{2\pi} \frac{F_l(\eta_p, pr_{<})}{pr_{<}} \frac{H_l^{(+)}(\eta_p, pr_{>})}{pr_{>}}, \quad (14)$$

where $\sigma_l = \sqrt{\Gamma(l+1+i\eta_p)/\Gamma(l+1-i\eta_p)}$ indicates the pure Coulomb phase shift and P_l denotes the Legendre function. $r_{<}$ ($r_{>}$) corresponds to the lesser (greater) of the coordinates r, r' and

$$F_l(\eta_p, \rho) = C_l(\eta_p) 2^{-l-1} (-i)^{l+1} M_{i\eta_p, l+1/2}(2i\rho), \quad (15)$$

$$H_l^{(+)}(\eta_p, \rho) = (-i)^l e^{\pi\eta_p/2} e^{i\sigma_l} W_{-i\eta_p, l+1/2}(-2i\rho), \quad (16)$$

with the conventionally defined the Whittaker functions $M_{k,\mu}(z)$ and $W_{k,\mu}(z)$. The normalized constant $C_l(\eta_p)$ is always positive and has the form

$$C_l^2(\eta_p) = \frac{2^{2l} C_0^2(\eta_p) \prod_{n=1}^l (n^2 + \eta_p^2)}{\Gamma(2l+2)^2} = 2^l e^{-\pi\eta_p/2} \frac{|\Gamma(l+1+i\eta_p)|}{\Gamma(2l+2)}, \quad (17)$$

where $C_0^2(\eta_p)$, the probability of finding the deuteron and alpha particles at zero separation, is defined as

$$C_0^2(\eta_p) = \chi_{p'}^{(\pm)}(\mathbf{0}) \chi_p^{*(\pm)}(\mathbf{0}) = \frac{2\pi\eta_p}{e^{2\pi\eta_p} - 1}. \quad (18)$$

The Coulomb Green's function for ${}^6\text{Li}$ bound state with two-body binding energy B is defined as

$$G_C^{(l)}(-B, r', r) = -\frac{i\mu\gamma}{2\pi} \frac{F_l(\eta_{i\gamma}, i\gamma r')}{i\gamma r'} \frac{H_l^{(+)}(\eta_{i\gamma}, i\gamma r)}{i\gamma r}, \quad (19)$$

where $\gamma = \sqrt{2\mu B}$ indicates the two-body binding momentum of ${}^6\text{Li}$ and the coordinate space definitions are as $r' < r$.

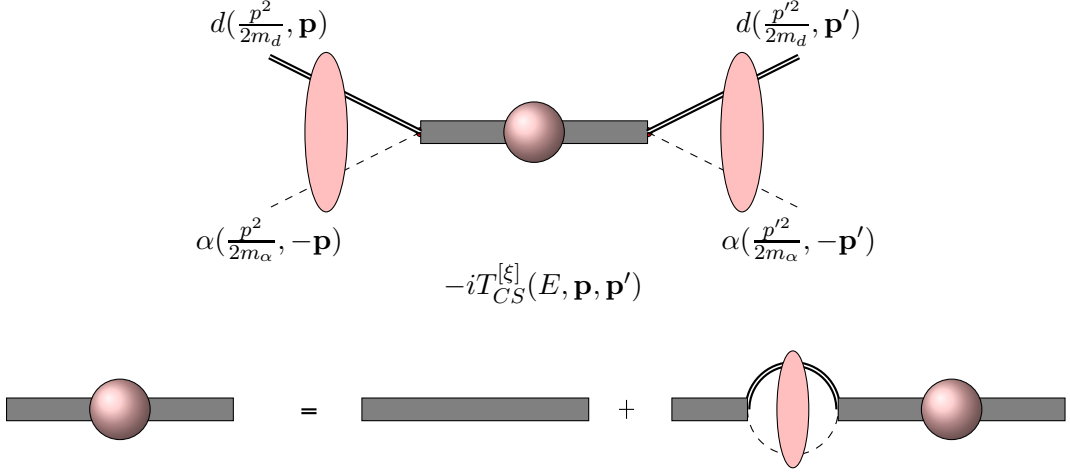


FIG. 2: The amplitude of the $d-\alpha$ elastic scattering. The thick line is the bare dimeron propagator and the thick dashed line with a filled circle represents the full dimeron propagator. All remained notations are the same as Fig. 1.

III. ELASTIC SCATTERING

The elastic scattering amplitude for two particles interacting via short-range strong and long-range Coulomb interactions in the CM framework can be written as [35]

$$T(\mathbf{p}', \mathbf{p}; E) = T_C(\mathbf{p}', \mathbf{p}; E) + T_{CS}(\mathbf{p}', \mathbf{p}; E), \quad (20)$$

where T_C indicates the pure Coulomb scattering amplitude and T_{CS} represents the scattering amplitude for the strong interaction in the presence of the Coulomb interaction with $E = p^2/2\mu$ as the CM energy of the system. \mathbf{p} and \mathbf{p}' denote the relative momentum of incoming and outgoing particles, respectively. These amplitudes can be expressed in the partial wave decomposition as [33]

$$T_C(\mathbf{p}', \mathbf{p}; E) = \sum_{l=0}^{\infty} (2l+1) T_C^{[l]} P_l(\hat{\mathbf{p}}' \cdot \hat{\mathbf{p}}) = -\frac{2\pi}{\mu} \sum_{l=0}^{\infty} (2l+1) \frac{e^{2i\sigma_l} - 1}{2ip} P_l(\hat{\mathbf{p}}' \cdot \hat{\mathbf{p}}), \quad (21)$$

and

$$T_{CS}(\mathbf{p}', \mathbf{p}; E) = \sum_{l=0}^{\infty} (2l+1) T_{CS}^{[l]}(p) e^{2i\sigma_l} P_l(\hat{\mathbf{p}}' \cdot \hat{\mathbf{p}}), \quad (22)$$

with

$$T_{CS}^{[l]}(p) = -\frac{2\pi}{\mu} \frac{1}{p(\cot\delta_l - i)}, \quad (23)$$

where δ_l denotes the Coulomb-corrected phase shift.

At low-energy $d - \alpha$ elastic scattering, the S -, P - and D -wave channels ($\xi = {}^3S_1, {}^3P_0, {}^3P_1, {}^3P_2, {}^3D_1, {}^3D_2, {}^3D_3$) dominantly contribute in the elastic scattering cross section. The CEFT diagram of the $d - \alpha$ elastic scattering amplitude is shown in Fig. 2. According to this diagram, the on-shell Coulomb-subtracted EFT amplitudes for each channel ξ can be obtained as [29]

$$-i(2l+1)T_{CS}^{[\xi]}(p) = -ig^{[\xi]^2} D^{[\xi]}(E, \mathbf{0}) C_0^2(\eta_p) W_l(\eta_p), \quad (24)$$

with the full dimer propagator for channel ξ as

$$D^{[\xi]}(E, \mathbf{0}) = \frac{\eta^{[\xi]}}{E - \Delta^{[\xi]} + h^{[\xi]} E^2 - \frac{1}{2l+1} \eta^{[\xi]} g^{[\xi]^2} J_l(E)}. \quad (25)$$

On the other hand, the on-shell Coulomb-subtracted amplitude $T_{CS}^{[\xi]}$ can usually be expressed in terms of a modified effective range expansion (ERE) as [36]

$$T_{CS}^{[\xi]}(p) = -\frac{2\pi}{\mu} \frac{C_0^2(\eta_p) W_l(\eta_p)}{K^{[\xi]}(p) - H_l(\eta_p)}, \quad (26)$$

with

$$W_l(\eta_p) = \frac{k_C^{2l}}{(l!)^2} \prod_{n=0}^l \left(1 + \frac{n^2}{\eta_p^2}\right), \quad (27)$$

$$H_l(\eta_p) = 2k_C W_l(\eta_p) H(\eta_p), \quad (28)$$

$$H(\eta_p) = \psi(i\eta_p) + \frac{1}{2i\eta_p} - \ln(i\eta_p), \quad (29)$$

where the function ψ is the logarithmic derivative of Gamma function. The function $K^{[\xi]}(p)$ represents the short-range strong interaction which is obtained in terms of the effective range parameters as [37]

$$K^{[\xi]}(p) = -\frac{1}{a^{[\xi]}} + \frac{1}{2} r^{[\xi]} p^2 + \frac{1}{4} s^{[\xi]} p^4 + \dots, \quad (30)$$

with $a^{[\xi]}$, $r^{[\xi]}$ and $s^{[\xi]}$ as the scattering length, effective range, and shape parameter, respectively.

The fully dressed bubble J_l in Eq. 25, is divergent and should be regularized. We can regularize the divergence by dividing the integral J_l into two finite and infinite parts as $J_l = J_l^{fin} + J_l^{div}$. The finite part is obtained as [38, 39]

$$J_l^{fin}(p) = -\frac{\mu}{2\pi} H_l(\eta_p). \quad (31)$$

The divergent parts absorb the $\Delta^{[\xi]}$, $g^{[\xi]}$ and $h^{[\xi]}$ parameters by introducing the renormalized parameters $\Delta_R^{[\xi]}$, $g_R^{[\xi]}$ and $h_R^{[\xi]}$. The details of these regularization and renormalization for all channels are presented in our previous paper [29]. Thus, comparing Eq. 24 to Eq. 26 yields

$$\Delta_R^{[\xi]} = -\frac{\mu\eta^{[\xi]}g_R^{[\xi]^2}}{(2l+1)2\pi a^{[\xi]}}, \quad g_R^{[\xi]^2} = -\frac{(2l+1)2\pi}{\mu^2\eta^{[\xi]}r^{[\xi]}}, \quad h_R^{[\xi]} = -\frac{\mu^3g_R^{[\xi]^2}s^{[\xi]}}{(2l+1)2\pi}. \quad (32)$$

At the binding energy of the ground state of ${}^6\text{Li}$, the amplitude should have a pole at the binding momentum $i\gamma$. Thus, we have

$$-\frac{1}{a^{[3S_1]}} - \frac{1}{2}r^{[3S_1]}\gamma^2 + \frac{1}{4}s^{[3S_1]}\gamma^4 + \dots - H_0(i\gamma) = 0. \quad (33)$$

By imposing this condition, the effective range parameter $a^{[3S_1]}$ is related to other effective range parameters which can be fixed by available experimental phase shift data of the elastic $d - \alpha$ scattering. The renormalization constant of the ${}^6\text{Li}$ wave function which is treated as a bound state of alpha and deuteron clusters is defined by the dressed S -wave dimer propagator as

$$\begin{aligned} \frac{1}{\mathcal{Z}} &= \frac{\partial D^{[3S_1]}(E, \mathbf{0})^{-1}}{\partial E} \Big|_{E=-B} \\ &= -\frac{g^{[3S_1]^2}\mu^2}{2\pi p} \frac{\partial}{\partial p} \left(\frac{1}{2}r^{[3S_1]}(p^2 + \gamma^2) + \frac{1}{4}s^{[3S_1]}(p^4 - \gamma^4) + \dots - H_0(\eta_p) + H_0(i\gamma) \right) \Big|_{p=i\gamma}. \end{aligned} \quad (34)$$

IV. $E1$ AND $E2$ TRANSITION AMPLITUDES

In this section, we focus on the calculation of the $E1$ and $E2$ transition amplitudes for the capture process $d(\alpha, \gamma){}^6\text{Li}$. First, the Feynman diagrams of one- and two-body currents that contribute to the dominant transitions ($E1$ and $E2$) are presented. Then, based on the Feynman rules, the transition amplitudes of diagrams for all possible partial waves ξ , are presented. As has been mentioned, α and d are considered as the point-like nuclei and the ${}^6\text{Li}$ is the two-body cluster bound state constructed by α and d . We assign the initial CM momentum \mathbf{p} for the $d - \alpha$ system and the outgoing photon in the final state denoted by \mathbf{k} .

In the low-energy regime, $p \leq k_C \sim 18$ MeV, the on-shell CM momentum of the system is scaled as low-momentum Q . The high-momentum scale is set by the lowest energy degrees of freedom that has been integrated out. According to the fact that there is no existing

explicit pions and any deuteron deformation, the high-momentum scale Λ has been chosen between the pion mass, $m_\pi \sim 140$ MeV and the momentum corresponding to the deuteron binding energy, B_d i.e., $\sqrt{2m_d B_d} \sim 90$ MeV. Around the $p \sim k_C \sim 18$ MeV, the expansion parameter of the current EFT is estimated to be of the order $1/5$. By increasing the energy, the expansion deteriorates and the precision of our EFT prediction will be questionable for $E_{CM} = p^2/(2\mu) > 3.3$ MeV. The Sommerfeld parameter η_p is enhanced by decreasing the energy. So, η_p would be large around $p \lesssim k_C$ and the elastic scattering and capture amplitudes require nonperturbative treatment of the Coulomb photons.

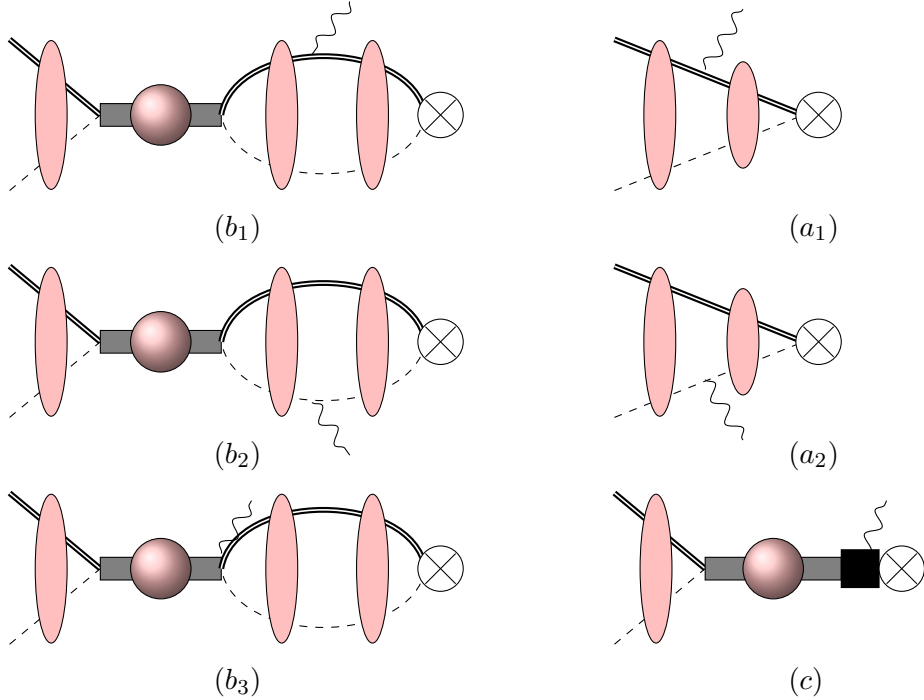


FIG. 3: Diagrams for the radiative capture process $d(\alpha, \gamma)^6\text{Li}$. The dashed and double lines represent the scalar α and vector deuteron particles respectively. The wavy line indicates the outgoing photon. The square depicts the two-body currents and the \otimes is the final bound state symbol.

According to the power counting, $\mu \sim \Lambda^3/Q^2$ and $\gamma \sim 3Q$. Thus, the energy-momentum conservation and EFT power counting yield

$$k = \frac{p^2 + \gamma^2}{2\mu} \sim \frac{Q^3}{\Lambda^2} \ll Q \sim p. \quad (35)$$

Thus, in the loop calculation, we can use this approximation:

$$E_d + k_0 + q_0 - \frac{(\mathbf{q} + \mathbf{k} + \mathbf{p})^2}{2m_d} \approx E_d + k_0 + q_0 - \frac{(\mathbf{q} + \mathbf{p})^2}{2m_d} \sim \frac{Q^2}{\mu} \sim \frac{Q^4}{\Lambda^3}, \quad (36)$$

with $E_d = p^2/(2m_d)$. (q_0, \mathbf{q}) and (k_0, \mathbf{k}) are the loop and photon energy-momentum, respectively. This approximation corresponds to the zero-recoil of the final bound state ${}^6\text{Li}$. Consequently, we disregard the recoil effect in our calculations up to next-to-next-to-leading order (N^2LO).

The Feynman diagrams that contribute to the $d(\alpha, \gamma){}^6\text{Li}$ process are shown in Fig. 3. The diagrams a_1 and a_2 are the possible transitions including only Coulomb interactions for the incoming charged particles. The diagrams b_1 , b_2 , and b_3 involve the initial state short-range interactions. In these diagrams, the external photon minimally couples to one of the single-charged particle lines. The last diagram, c , denotes the contribution of the two-body current in the gamma capture process. The $E1$ transition amplitude through all possible incoming P - waves is written as

$$M_{E1}(\mathbf{p}) = \sum_{\xi=3P_0, 3P_1, 3P_2} \left(M_{E1,a1,2}^{[\xi]}(\mathbf{p}) + M_{E1,b1,2}^{[\xi]}(\mathbf{p}) + M_{E1,b3}^{[\xi]}(\mathbf{p}) + M_{E1,c}^{[\xi]}(\mathbf{p}) \right). \quad (37)$$

As shown in the following, this amplitude leads to

$$M_{E1}(\mathbf{p}) = \mathcal{M}_{E1}(p) \varepsilon_i^d \varepsilon_j^{Li*} (\boldsymbol{\varepsilon}^{\gamma*} \cdot \hat{\mathbf{p}}), \quad (38)$$

where $\boldsymbol{\varepsilon}^\gamma$ denotes the polarization vector of the outgoing photon and $\boldsymbol{\varepsilon}^d$ and $\boldsymbol{\varepsilon}^{Li}$ are spin polarization vectors of d and ${}^6\text{Li}$, respectively. The $E1$ transition amplitudes from the initial 3P_0 , 3P_1 , and 3P_2 states to the final bound state 3S_1 , corresponding to the diagrams a_1 , a_2 , b_1 , b_2 , b_3 and c are obtained as

$$\begin{aligned} M_{E1,a1,2}^{[\xi]}(\mathbf{p}) &= \frac{i}{\mu} Q_1 g^{[3S_1]} \sqrt{\mathcal{Z}} \varepsilon_i^d \varepsilon_j^{Li*} \varepsilon_k^{\gamma*} \int d^3r G_C^{(0)}(-B, 0, r) \nabla_k [3P_1(\hat{\mathbf{p}} \cdot \hat{\mathbf{r}}) \chi_p^{(1)}(r)] \\ &= 2 Q_1 g^{[3S_1]} \sqrt{\mathcal{Z}} C_0(\eta_p) e^{i\sigma_1} \mathcal{A}_1(p) \varepsilon_i^d \varepsilon_j^{Li*} (\boldsymbol{\varepsilon}^{\gamma*} \cdot \hat{\mathbf{p}}), \end{aligned} \quad (39)$$

$$\begin{aligned}
M_{E1,b_{1,2}}^{[\xi]}(\mathbf{p}) &= \frac{1}{\mu} Q_1 g^{[3S_1]} \sqrt{\mathcal{Z}} \varepsilon_i^d \varepsilon_j^{Li*} \varepsilon_k^{\gamma*} \frac{3T_{CS}^{[\xi]}(p) e^{i\sigma_1}}{C_0(\eta_p) W_1^{1/2}(\eta_p)} \hat{\mathbf{p}}_l \\
&\quad \times \int d^3r G_C^{(0)}(-B, 0, r) \lim_{\mathbf{r}'' \rightarrow 0} \nabla_k \nabla_l'' [3P_1(\hat{\mathbf{r}} \cdot \hat{\mathbf{r}}'') G_C^{(1)}(E, r, r'')] \\
&= 2 Q_1 g^{[3S_1]} \sqrt{\mathcal{Z}} \frac{C_0(\eta_p) W_1^{1/2}(\eta_p)}{K^{[\xi]}(p) - H_1(\eta_p)} e^{i\sigma_1} \mathcal{B}_1(p) \varepsilon_i^d \varepsilon_j^{Li*} (\boldsymbol{\varepsilon}^{\gamma*} \cdot \hat{\mathbf{p}}), \tag{40}
\end{aligned}$$

$$\begin{aligned}
M_{E1,b_3}^{[\xi]}(\mathbf{p}) &= i Q_1 g^{[3S_1]} \sqrt{\mathcal{Z}} \varepsilon_i^d \varepsilon_j^{Li*} \varepsilon_k^{\gamma*} G_C^{(0)}(-B, 0, 0) \frac{3T_{CS}^{[\xi]}(p) e^{i\sigma_1}}{C_0(\eta_p) W_1^{1/2}(\eta_p)} \hat{\mathbf{p}}_k \\
&= -\frac{6\pi i}{\mu} Q_1 g^{[3S_1]} \sqrt{\mathcal{Z}} \frac{C_0(\eta_p) W_1^{1/2}(\eta_p)}{K^{[\xi]}(p) - H_1(\eta_p)} e^{i\sigma_1} J_0(i\gamma) \varepsilon_i^d \varepsilon_j^{Li*} (\boldsymbol{\varepsilon}^{\gamma*} \cdot \hat{\mathbf{p}}), \tag{41}
\end{aligned}$$

$$\begin{aligned}
M_{E1,c}^{[\xi]}(\mathbf{p}) &= i\mu k_0 Q_1 g^{[3S_1]} \sqrt{\mathcal{Z}} \varepsilon_i^d \varepsilon_j^{Li*} \varepsilon_k^{\gamma*} L_{E1} \frac{3T_{CS}^{[\xi]}(p) e^{i\sigma_1}}{C_0(\eta_p) W_1^{1/2}(\eta_p)} \hat{\mathbf{p}}_k \\
&= -6i\pi k_0 L_{E1} Q_1 g^{[3S_1]} \sqrt{\mathcal{Z}} \frac{C_0(\eta_p) W_1^{1/2}(\eta_p)}{K^{[\xi]}(p) - H_1(\eta_p)} e^{i\sigma_1} \varepsilon_i^d \varepsilon_j^{Li*} (\boldsymbol{\varepsilon}^{\gamma*} \cdot \hat{\mathbf{p}}). \tag{42}
\end{aligned}$$

with

$$\mathcal{A}_1(p) = \frac{\Gamma(1+k_C/\gamma)}{C_0(\eta_p)} \int_0^\infty dr r W_{-k_C/\gamma, 1/2}(2\gamma r) \left(3 + r \frac{\partial}{\partial r}\right) \frac{F_1(\eta_p, pr)}{pr^2}, \tag{43}$$

$$\mathcal{B}_1(p) = ip \Gamma(1+k_C/\gamma) \Gamma(2+i\eta_p) \int_0^\infty dr r W_{-k_C/\gamma, 1/2}(2\gamma r) \left(\frac{2}{r} + \frac{\partial}{\partial r}\right) \frac{W_{-i\eta_p, 3/2}(-2ipr)}{r}. \tag{44}$$

We are working in Coulomb gauge where the relation $\boldsymbol{\varepsilon}^\gamma \cdot \mathbf{k} = 0$ for the real photon with momentum \mathbf{k} is fulfilled. Also, the spherical symmetry $r_i r_j / r^2 \rightarrow \delta_{ij} / 3$ is used in the integrals of Eqs. 39 and 40. The Whittaker function $W_{-k_C/\gamma, 1/2}(2\gamma r)$, in diagrams a_1 , a_2 , b_1 and b_2 is associated with the final S -wave bound state wave function and the P -wave Coulomb wave function $F_1(\eta_p, pr)$ in a_1 and a_2 diagrams corresponds to the initial incoming scattering state [40]. Moreover, due to the presence of one bound-state field, there is a wave function renormalization $\sqrt{\mathcal{Z}}$ present. Thus, the $E1$ transition amplitude for the $d(\alpha, \gamma)^6\text{Li}$ process is summarized as

$$\mathcal{M}_{E1}(p) = 2 Q_1 g^{[3S_1]} \sqrt{\mathcal{Z}} C_0(\eta_p) e^{i\sigma_1} \left[\mathcal{A}_1(p) + \frac{W_1^{1/2}(\eta_p)}{K^{[\xi]}(p) - H_1(\eta_p)} \left(\mathcal{B}_1(p) - \frac{3\pi i}{\mu} J_0(i\gamma) - 3\pi i k_0 L_{E1} \right) \right]. \tag{45}$$

By increasing the CM energy, the $E2$ transition would be more important in the $d(\alpha, \gamma)^6\text{Li}$ reaction. So, we should consider the contribution of the $E2$ transition to include 3^+ resonance

at $E_{CM} = 0.711$ MeV. So, in the following, the $E2$ transition for $d(\alpha, \gamma)^6\text{Li}$ reaction which involves transition from 3D_1 , 3D_2 and 3D_3 to 3S_1 would be considered. The contribution of all diagrams in the $E2$ transition can be summarized as

$$M_{E2}(\mathbf{p}) = \sum_{\xi=^3D_1, ^3D_2, ^3D_3} (M_{E2,a_1,2}^{[\xi]}(\mathbf{p}) + M_{E2,b_1,2}^{[\xi]}(\mathbf{p}) + M_{E2,b_3}^{[\xi]}(\mathbf{p}) + M_{E2,c}^{[\xi]}(\mathbf{p})), \quad (46)$$

with

$$M_{E2}(\mathbf{p}) = \mathcal{M}_{E2}(p) \varepsilon_i^d \varepsilon_j^{Li*} (\hat{\mathbf{k}} \cdot \hat{\mathbf{p}}) (\boldsymbol{\varepsilon}^{\gamma*} \cdot \hat{\mathbf{p}}). \quad (47)$$

The $E2$ transition amplitude from the initial 3D_1 , 3D_2 , and 3D_3 states to the final bound state 3S_1 , for the diagrams a_1 , a_2 , b_1 , b_2 and b_3 are obtained as

$$\begin{aligned} M_{E2,a_1,2}^{[\xi]}(\mathbf{p}) &= -\frac{1}{\mu} Q_2 g^{[3S_1]} \sqrt{\mathcal{Z}} \varepsilon_i^d \varepsilon_j^{Li*} \varepsilon_k^{\gamma*} k_l \int d^3r G_C^{(0)}(-B, 0, r) r_l \nabla_k [5P_2(\hat{\mathbf{p}} \cdot \hat{\mathbf{r}}) \chi_p^{(2)}(r)], \\ &= -2k Q_2 g^{[3S_1]} \sqrt{\mathcal{Z}} e^{i\sigma_2} \mathcal{A}_2(p) \varepsilon_i^d \varepsilon_j^{Li*} (\hat{\mathbf{k}} \cdot \hat{\mathbf{p}}) (\boldsymbol{\varepsilon}^{\gamma*} \cdot \hat{\mathbf{p}}), \end{aligned} \quad (48)$$

$$\begin{aligned} M_{E2,b_1,2}^{[\xi]}(\mathbf{p}) &= \frac{i}{\mu} Q_2 g^{[3S_1]} \sqrt{\mathcal{Z}} \varepsilon_i^d \varepsilon_j^{Li*} \varepsilon_k^{\gamma*} \frac{5T_{CS}^{[\xi]}(p) e^{i\sigma_2}}{C_0(\eta_p) W_2^{1/2}(\eta_p)} (\hat{\mathbf{p}}_n \hat{\mathbf{p}}_m - \frac{1}{3} \delta_{nm}) k_l \int d^3r \\ &\quad \times G_C^{(0)}(-B, 0, r) r_l \nabla_k \lim_{\mathbf{r}'' \rightarrow 0} (\nabla_n'' \nabla_m'' - \frac{1}{3} \delta_{nm} \nabla_n'' \nabla_m'') [5P_2(\hat{\mathbf{r}} \cdot \hat{\mathbf{r}}'') G_C^{(2)}(E, r, r'')] \\ &= -\frac{2i}{3} k Q_2 g^{[3S_1]} \sqrt{\mathcal{Z}} \frac{C_0(\eta_p) W_2^{1/2}(\eta_p)}{K^{[\xi]}(p) - H_2(\eta_p)} e^{i\sigma_2} \mathcal{B}_2(p) \varepsilon_i^d \varepsilon_j^{Li*} (\hat{\mathbf{k}} \cdot \hat{\mathbf{p}}) (\boldsymbol{\varepsilon}^{\gamma*} \cdot \hat{\mathbf{p}}), \end{aligned} \quad (49)$$

$$\begin{aligned} M_{E2,b_3}^{[\xi]}(\mathbf{p}) &= -Q_2 g^{[3S_1]} \sqrt{\mathcal{Z}} \varepsilon_i^d \varepsilon_j^{Li*} \varepsilon_k^{\gamma*} k_l G_C^{(0)}(-B, 0, 0) \frac{5T_{CS}^{[\xi]}(p) e^{i\sigma_2}}{C_0(\eta_p) W_2^{1/2}(\eta_p)} (\hat{\mathbf{p}}_k \hat{\mathbf{p}}_l - \frac{1}{3} \delta_{kl}) \\ &= \frac{10\pi}{\mu} k Q_2 g^{[3S_1]} \sqrt{\mathcal{Z}} \frac{C_0(\eta_p) W_2^{1/2}(\eta_p)}{K^{[\xi]}(p) - H_2(\eta_p)} e^{i\sigma_2} J_0(i\gamma) \varepsilon_i^d \varepsilon_j^{Li*} (\hat{\mathbf{k}} \cdot \hat{\mathbf{p}}) (\boldsymbol{\varepsilon}^{\gamma*} \cdot \hat{\mathbf{p}}), \end{aligned} \quad (50)$$

$$\begin{aligned} M_{E2,c}^{[\xi]}(\mathbf{p}) &= -\mu Q_2 g^{[3S_1]} \sqrt{\mathcal{Z}} \varepsilon_i^d \varepsilon_j^{Li*} L_{E1} k_0 \varepsilon_k^{\gamma*} k_l \frac{5T_{CS}^{[\xi]}(p) e^{i\sigma_2}}{C_0(\eta_p) W_2^{1/2}(\eta_p)} (\hat{\mathbf{p}}_k \hat{\mathbf{p}}_l - \frac{1}{3} \delta_{kl}) \\ &= 10\pi k k_0 Q_2 g^{[3S_1]} \sqrt{\mathcal{Z}} L_{E2} \frac{C_0(\eta_p) W_2^{1/2}(\eta_p)}{K^{[\xi]}(p) - H_2(\eta_p)} e^{i\sigma_2} \varepsilon_i^d \varepsilon_j^{Li*} (\hat{\mathbf{k}} \cdot \hat{\mathbf{p}}) (\boldsymbol{\varepsilon}^{\gamma*} \cdot \hat{\mathbf{p}}), \end{aligned} \quad (51)$$

with

$$\mathcal{A}_2(p) = \frac{\Gamma(1 + \frac{kc}{\gamma})}{C_0(\eta_p)} \int_0^\infty dr r^2 W_{-kc/\gamma, 1/2}(2\gamma r) \left(\frac{3}{r} + \frac{\partial}{\partial r} \right) \frac{F_2(\eta_p, pr)}{pr}, \quad (52)$$

$$\mathcal{B}_2(p) = -p^2 \Gamma(1 + \frac{kc}{\gamma}) \Gamma(3 + i\eta_p) \int_0^\infty dr r^2 W_{-kc/\gamma, 1/2}(2\gamma r) \left(\frac{3}{r} + \frac{\partial}{\partial r} \right) \frac{W_{-i\eta_p, 5/2}(-2ipr)}{r}. \quad (53)$$

Spherical symmetry is used to write $r_k r_j r_i r_l / r^4 \rightarrow (\delta_{kj} \delta_{il} + \delta_{ki} \delta_{jl} + \delta_{kl} \delta_{ji}) / 15$ in the integrals. Thus, the $E2$ transition amplitude for the $d(\alpha, \gamma)^6\text{Li}$ capture reaction from the initial D -wave states is summarized as

$$\mathcal{M}_{E2}^{[\xi]}(p) = -2k Q_2 g^{[{}^3S_1]} \sqrt{\mathcal{Z}} C_0(\eta_p) e^{i\sigma_2} \times \left[\mathcal{A}_2(p) + \frac{W_2^{1/2}(\eta_p)}{K^{[\xi]}(p) - H_2(\eta_p)} \left(\frac{i}{3} \mathcal{B}_2(p) - \frac{5\pi}{\mu} J_0(i\gamma) - 5\pi k_0 L_{E2} \right) \right]. \quad (54)$$

The loops of the diagrams b_1 and b_2 lead to a logarithmic divergence in $M_{E1, b_{1,2}}^{[\xi]}$ and $M_{E2, b_{1,2}}^{[\xi]}$ amplitudes when r goes to zero. A short-range cutoff r_C in the r integral in Eqs. 44 and 53 is introduced as a regulator and the divergence can be handled by renormalizing the counter terms L_{E1} and L_{E2} [41], [42]. The loop of the diagram b_3 is also divergent and could be renormalized by the L_{E1} and L_{E2} terms as well. By extracting the divergent parts, the renormalized L_{E1} and L_{E2} can be expressed as

$$L_{E1}^R = L_{E1} + \frac{1}{\mu k_0} \left[J_0^{div} + \frac{i\mu}{3\pi} \mathcal{B}_1^{div} \right], \quad (55)$$

$$L_{E2}^R = L_{E2} + \frac{1}{\mu k_0} \left[J_0^{div} - \frac{i\mu}{15\pi} \mathcal{B}_2^{div} \right], \quad (56)$$

with

$$\mathcal{B}_1^{div} = \mathcal{B}_2^{div} = k_C \int_0^{r_C} \frac{dr}{r} \rightarrow k_C \left(\frac{\kappa}{2} \right)^{2\epsilon} \int_0^{r_C} \frac{dr}{r^{1-2\epsilon}} = k_C \left[\frac{1}{2\epsilon} + \ln\left(\frac{\kappa}{2} r_C\right) + \mathcal{O}(\epsilon) \right]. \quad (57)$$

In the power divergence subtraction (PDS) regularization scheme, the divergent part of J_0 that does not depend on the momentum is obtained as [43]

$$J_0^{div} = \frac{\mu k_C}{2\pi} \left[\frac{1}{\epsilon} + \ln\left(\frac{\pi \kappa^2}{4k_C^2}\right) + 2 - 3C_E \right], \quad (58)$$

with D the dimensionality of spacetime, κ the renormalization mass scale and $C_E = 0.577\dots$ Euler–Mascheroni constant. The L_{E1}^R and L_{E2}^R refer to the renormalized parameters that have been adjusted with fitting to the astrophysical S-factor experimental data.

V. RESULTS

The astrophysical S-factor plays a crucial role in the nuclear fusion reactions in the core of stars. This factor allows us to calculate how quickly those reactions take place, taking into account the interaction between the reacting particles. It defines as

$$S(E) \equiv E \exp(2\pi\eta_p) \sigma(p), \quad (59)$$

where $E = p^2/2\mu$ is the CM energy of system and $\sigma(p)$ denotes the total cross-section. The differential cross section for our reaction is calculated by averaging over the initial spin and summing over all components of the final state i.e., the outgoing photon polarization and the ${}^6\text{Li}$ spin components as

$$\frac{d\sigma}{d\Omega} = \frac{\mu k}{8\pi^2 p} \frac{1}{9} \sum_{i,j=1}^3 \sum_{r=1}^2 \left| [\mathcal{M}_{E1}(p) + \mathcal{M}_{E2}(p)(\hat{\mathbf{k}} \cdot \hat{\mathbf{p}})] (\boldsymbol{\varepsilon}_r^{\gamma*} \cdot \hat{\mathbf{p}}) \varepsilon_i^d \varepsilon_j^{Li*} \right|^2, \quad (60)$$

by considering photon momentum direction $\hat{\mathbf{k}}$ along \hat{z} axis and integrating over angle variables, the total cross section is presented by

$$\sigma(p) = \frac{\mu k}{18\pi p} \left(|\mathcal{M}_{E1}(p)|^2 + \frac{1}{5} |\mathcal{M}_{E2}(p)|^2 \right). \quad (61)$$

To calculate the S-factor using the EFT expressions for the $E1$ and $E2$ transition amplitudes of Eqs. 45 and 54, we need to determine the values of the elastic P - and D - waves scattering parameters and the $E1$ and $E2$ two-body coupling constants. We recently obtained S -, P -, and D -wave scattering parameters by phase shift analysis in our previous paper [29]. For the $E1$ and $E2$ two-body coupling constants L_{E1}^R and L_{E2}^R , we have matched our EFT relation for the S-factor to the available experimental data [1, 18–22] at the energy range 0.001 – 3.3 MeV with arbitrary values of the cutoff r_C . Table II shows the results of the S-factor in energies $E_{CM} = 0.2$ and 3 MeV as a function of r_C . The L_{E1}^R and L_{E2}^R constants and S-factor demonstrate a notable correlation with the short-range cutoff r_C . As the radius r_C decreases, the S-factor increases gradually. It can be seen that for the cutoff values below $r_C = 0.1$ fm, the S-factor values would be stable. This indicates the insensitivity of the S-factor to the precisely chosen short-range cutoff within the region of $r_C \leq 0.1$ fm.

According to the power counting proposed in Sec. IV, the dominant contributions of the scattering amplitude in channels 3P_0 , 3P_1 , 3P_2 , 3D_1 and 3D_2 come clearly from their scattering lengths and the influences of both their effective ranges and shape parameters are small and can be considered as higher-order corrections [29]. Based on this power counting, the effective charges Q_1 and Q_2 scale as Q^4/Λ^4 and Q/Λ , respectively. We also consider $\mathcal{B}_2/\mathcal{A}_2 \sim \Lambda^4/Q^2$ and $\mathcal{B}_1/\mathcal{A}_1 \sim Q^2\Lambda$ which hold over a range of $0.1 \lesssim E_{CM} \lesssim 3.3$ MeV. Taking into account these analyses, we can estimate the order of all diagrams in both $E1$ and $E2$ transition amplitudes for each channel. In Table III, the relative contribution of diagrams $b_{1,2}$, b_3 and c for each channel to the diagrams $a_{1,2}$ in channel 3D_3 are presented. It is shown the leading-order contribution comes from the diagrams b_3 and c in the 3D_3 channel that

TABLE II: Fitted values of the L_{E1}^R and L_{E2}^R constants to experimental data of S-factor at $E_{CM} = 0.001 - 3.3$ MeV with the cutoff $r_C = 0.001 - 1$ fm. In the fourth and the last columns, the results of S-factor at $E_{CM} = 0.2$ MeV and $E_{CM} = 3$ MeV are presented.

r_C (fm)	L_{E1}^R	L_{E2}^R	S-factor(MeV.b) ($E_{CM} = 0.2$ MeV)	S-factor(MeV.b) ($E_{CM} = 3$ MeV)
1	$(5.805 \pm 0.881) \times 10^{-1}$	2.197 ± 0.383	4.841×10^{-9}	3.271×10^{-7}
0.5	$(5.421 \pm 0.732) \times 10^{-1}$	1.945 ± 0.326	4.985×10^{-9}	3.724×10^{-7}
0.2	$(5.187 \pm 0.865) \times 10^{-1}$	1.621 ± 0.293	5.171×10^{-9}	3.993×10^{-7}
0.1	$(4.942 \pm 0.719) \times 10^{-1}$	1.352 ± 0.318	5.312×10^{-9}	4.083×10^{-7}
0.05	$(4.733 \pm 0.748) \times 10^{-1}$	1.349 ± 0.304	5.319×10^{-9}	4.101×10^{-7}
0.001	$(4.721 \pm 0.752) \times 10^{-1}$	1.344 ± 0.315	5.320×10^{-9}	4.103×10^{-7}

TABLE III: The relative contribution of diagrams $b_{1,2}$, b_3 , c for each channel to the diagrams $a_{1,2}$ for channel 3D_3 around the resonance energy $E_{CM} = 0.71$ MeV, according to the suggested power counting.

ξ	$\mathcal{M}_{E1,a1,2}^{[\xi]}/\mathcal{M}_{E2,a1,2}^{[\xi]}$	$\mathcal{M}_{E1,b1,2}^{[\xi]}/\mathcal{M}_{E2,a1,2}^{[\xi]}$	$\mathcal{M}_{E1,b3}^{[\xi]}/\mathcal{M}_{E2,a1,2}^{[\xi]}$	$\mathcal{M}_{E1,c}^{[\xi]}/\mathcal{M}_{E2,a1,2}^{[\xi]}$
3P_0	Q/Λ	Q/Λ	Q/Λ	Q/Λ
3P_1	Q/Λ	Q^2/Λ^2	Q^2/Λ^2	Q^2/Λ^2
3P_2	Q/Λ	Q^2/Λ^2	Q^2/Λ^2	Q^2/Λ^2
ξ	$\mathcal{M}_{E2,a1,2}^{[\xi]}/\mathcal{M}_{E2,a1,2}^{[\xi]}$	$\mathcal{M}_{E2,b1,2}^{[\xi]}/\mathcal{M}_{E2,a1,2}^{[\xi]}$	$\mathcal{M}_{E2,b3}^{[\xi]}/\mathcal{M}_{E2,a1,2}^{[\xi]}$	$\mathcal{M}_{E2,c}^{[\xi]}/\mathcal{M}_{E2,a1,2}^{[\xi]}$
3D_1	1	Q^4/Λ^4	Q/Λ	Q/Λ
3D_2	1	Q^4/Λ^4	Q/Λ	Q/Λ
3D_3	1	Q^2/Λ^2	Λ/Q	Λ/Q

can independently reproduce the resonance of the S-factor observed at $E_{CM} = 0.711$ MeV. Around the resonance energy, the $a_{1,2}$ diagrams for all D -waves can be considered as the next-to-leading-order corrections. Additionally, the b_3 and c diagrams corresponding to the 3D_1 and 3D_2 waves along with the $a_{1,2}$ diagrams for all P waves have N²LO contribution same as the $b_{1,2}$, b_3 and c diagrams for the 3P_0 channel. The remaining diagrams in Table III

are affected by S-factor as higher-order corrections.

In Fig. 4, the contributions of each partial wave in our EFT calculation for the astrophysical S-factor of the capture reaction $d(\alpha, \gamma)^6\text{Li}$ are presented. It shows that the primary contribution comes from the initial 3P_2 partial wave at energies below 0.1 MeV in the CM framework. Moving into the resonance region, the 3D_3 channel becomes the dominant contribution making the resonance at $E_{CM} = 0.711$ MeV. The EFT results indicated in Fig. 4 are in agreement with the power counting estimations in Table III. Also, the contributions of $E1$, $E2$, and the $E1 + E2$ transitions of the astrophysical S-factor for the capture reaction $d(\alpha, \gamma)^6\text{Li}$ are shown in Fig. 5.

In the two-body models, the $E1$ transition from P -waves to the ^6Li ground state is significantly hindered by the isospin selection rule for $N = Z$ nuclei due to the nearly identical charge-to-mass ratios of the deuteron and the α particle.

This appears as a large suppression factor $(Z_d/m_d - Z_\alpha/m_\alpha)$ in the $E1$ transition amplitude. According to the incoming alpha particle ($J^\pi = 0^+$ and $I = 0$) and the deuteron ($J^\pi = 1^+$ and $I = 0$) and also the final ^6Li nucleus in its ground state ($J^\pi = 1^+$ and $I = 0$), and considering the point-like treatments for the alpha and deuteron, the dominant iso-scalar part of the $E1$ transition only contributes in the calculation of the $E1$ transition amplitude. The iso-vector part comes from excited states of incoming particles or the final state, which can be considered at higher energy. Since there is no state of substructure for the deuteron as $n + p$ for the triplet isospin contribution, the $d - \alpha$ system's isospin is zero. Consequently, there is no isospin breaking in the current CEFT. Here, the effects of the isospin mixture can be considered in $d(\alpha, \gamma)^6\text{Li}$ by inclusion of the $n - ^5\text{Li}$ and $p - ^5\text{He}$ systems in the intermediate states at high energy.

At energies 4.19 MeV and 3.18 MeV above the $d - \alpha$ breakup threshold, the $n - ^5\text{Li}$ and $p - ^5\text{He}$ breakup channels respectively, are open. In this case, we might have introduced the $n - ^5\text{Li}$ and $p - ^5\text{He}$ fields as relevant degrees of freedom in the theory. The $n - ^5\text{Li}$ and $p - ^5\text{He}$ fields then appear in the intermediate states as $n - ^5\text{Li}$ and $p - ^5\text{He}$ propagation in the loop diagrams b_1 , b_2 , and b_3 instead of the $d - \alpha$ propagation. In our work, however, the $n - ^5\text{Li}$ and $p - ^5\text{He}$ fields are regarded as irrelevant degrees of freedom at high energy and are integrated out of the effective Lagrangian. This effect is embedded in the coefficient and the contact interaction L_{E1}^R in diagram c , which are fitted to the experimental data of the S-factor.

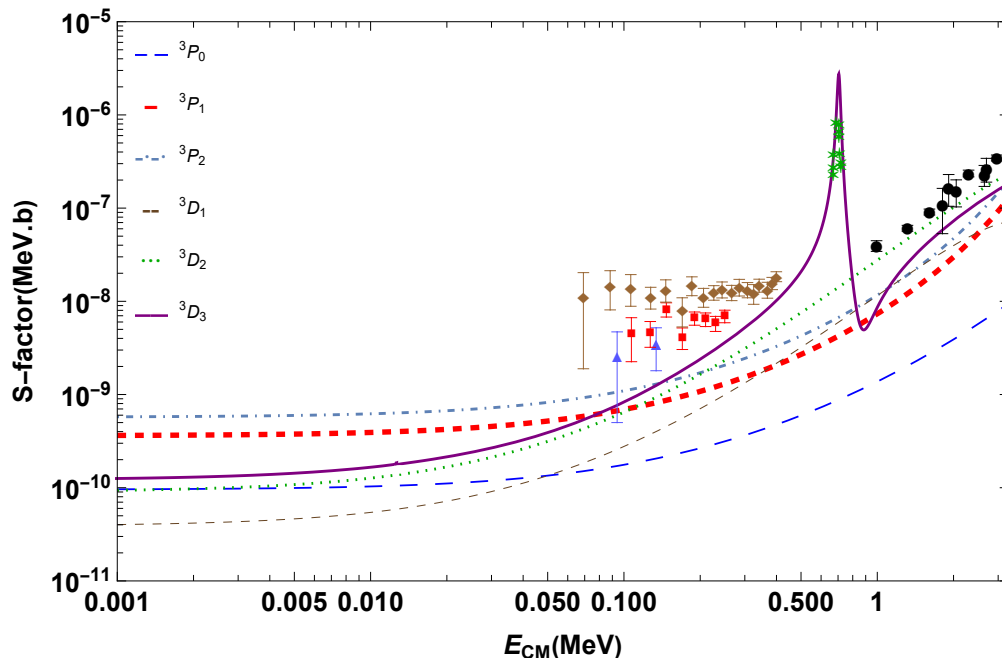


FIG. 4: Contributions of the different incoming partial waves components in our calculated EFT astrophysical S-factor for the capture reaction $d(\alpha, \gamma)^6\text{Li}$ compared with the experimental data of direct measurements: black circles [18], blue triangles[19], green stars [20], brown diamonds [21], red squares[22].

As we expect, the $E1$ capture will be more dominant than $E2$ capture at energies lower than 0.1 MeV due to the different energy dependencies of the penetration probabilities in the P - and D -waves. In contrast, the $E2$ component becomes more significant at energies related to the resonance energy and higher. At energies below 0.1 MeV, it is expected that $E1$ capture will be more dominant than $E2$ capture in the center-of-mass frame due to the distinct energy dependencies of the penetration probabilities in P - and D - waves [8]. Finally, the result obtained for astrophysical S-factor based on cluster EFT approach has been compared with the results obtained from two other theoretical approaches in Fig. 6 [9, 11].

VI. CONCLUSION

In this paper, we have studied the low-energy $d(\alpha, \gamma)^6\text{Li}$ gamma capture reaction with the two-body cluster EFT approach. Based on this approach, the deuteron and alpha nucleus

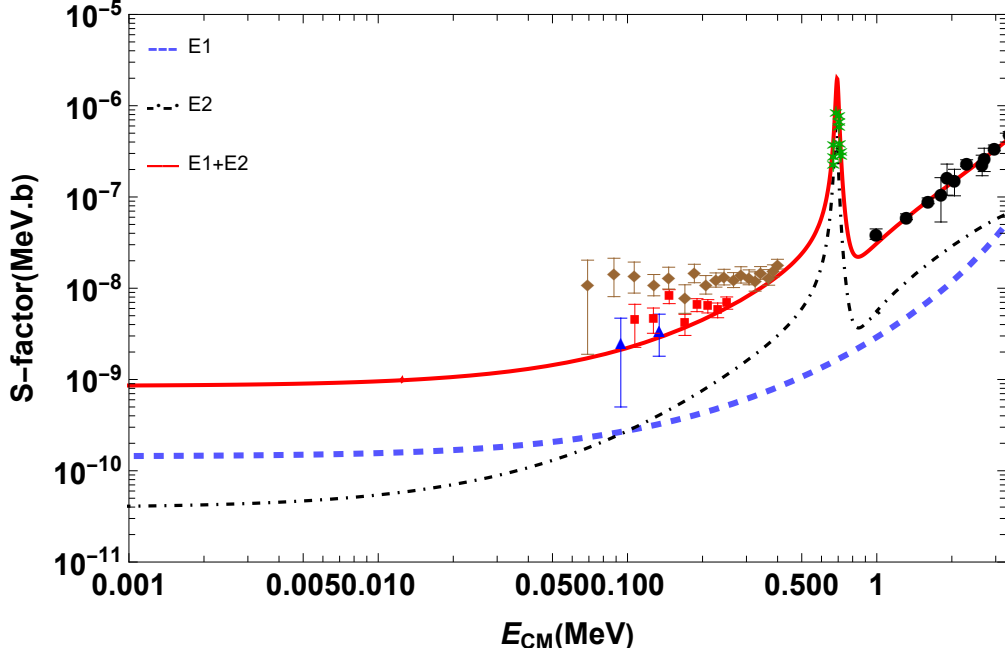


FIG. 5: The contribution of the $E1$ and $E2$, and the $E1 + E2$ transitions to the astrophysical S-factor for the capture reaction $d(\alpha, \gamma)^6\text{Li}$ according to our cluster effective field theory approach. In this figure, the order of each diagram is also shown. The experimental data are the same as Fig. 4.

are the point-like nuclear clusters and considering the fact that there are no existing explicit pions, we have concentrated on the energy region $E_{CM} \lesssim 3.3$ MeV. In this energy region, the Coulomb force was considered nonperturbatively. In the study of the radiative $d(\alpha, \gamma)^6\text{Li}$ capture reaction, we calculate the radiative capture amplitudes for the initial P - and D -waves of the $d - \alpha$ system. The Isoscaler component of $E1$ transition from initial P -wave states to the ground state of ^6Li was considered and the $E2$ transition contains D -wave initial states.

Our EFT results in Fig. 4 illustrate the significance of $l \leq 2$ partial waves in the astrophysical S-factor of the reaction where a deuterium nucleus captures an alpha particle to form ^6Li . It is evident that at energies below 0.1 MeV in the CM framework, the primary contribution comes from the initial 3P_2 partial wave. Moving into the resonance region, the 3D_3 channel becomes the dominant contribution, making the resonance at $E_{CM} = 0.711$ MeV. Below an energy threshold of 0.1 MeV in the CM frame, the primary influence stems from the initial 3P_2 partial wave.

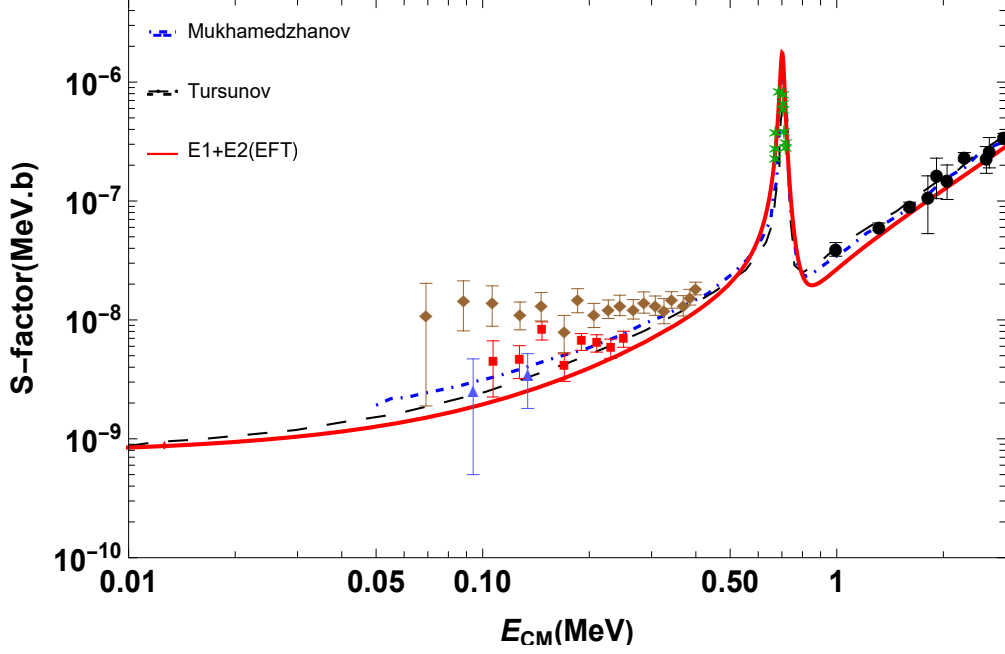


FIG. 6: Comparison of the result obtained for astrophysical S-factor from cluster EFT approach with the results obtained from two other theoretical approaches [9, 11].

Next, we analyzed the cluster Effective Field Theory results for the $E1$ and $E2$ contributions, contrasting them with existing experimental data. In Fig. 5, the $E1$, $E2$, and combined $E1+E2$ transitions of the astrophysical S-factor for the capture reaction $d(\alpha, \gamma)^6\text{Li}$ are represented. The primary role of the $E1$ transition is emphasized in the astrophysical S-factor of the gamma capture reaction $d(\alpha, \gamma)^6\text{Li}$ for energies below 0.1 MeV. Once the energy surpasses this threshold, the dominance shifts towards the $E2$ channel. It has been determined that the $E2$ transition, specifically through the two-body current diagram, plays a significant role in accurately capturing the resonance behavior observed at energies above 0.1 MeV.

In the current CEFT calculation, where the deuteron is assumed to be a point-like particle, the results for $E_{CM} > 3.3$ MeV are controversial. Employing the three-body cluster formalism is crucial for accurately understanding and calculating cross sections at higher energies. To resolve the disparities in the S-factor findings for CM energies exceeding 3.3 MeV, a three-body cluster effective field theory method can be utilized. This approach considers the neutron, proton, and alpha particles as relevant degrees of freedom.

Acknowledgment

This work is based upon research funded by the Iran National Science Foundation (INSF) under project No. 4003662. We are grateful to Dr. Ergash Tursunov for sharing the experimental data.

-
- [1] D. Trezzi, M. Anders, M. Aliotta, A. Bellini, D. Bemmerer, A. Boeltzig, C. Broggini, C. Bruno, A. Caciolli, F. Cavanna, et al., *Astroparticle Physics* **89**, 57 (2017).
 - [2] P. D. Serpico, S. Esposito, F. Iocco, G. Mangano, G. Miele, and O. Pisanti, *Journal of Cosmology and Astroparticle Physics* **2004**, 010 (2004).
 - [3] Y. a. Xu, K. Takahashi, S. Goriely, M. Arnould, M. Ohta, and H. Utsunomiya, *Nuclear Physics A* **918**, 61 (2013).
 - [4] K. Arai, D. Baye, and P. Descouvemont, *Nuclear Physics A* **699**, 963 (2002).
 - [5] L. Lamia, C. Spitaleri, R. Pizzone, E. Tognelli, A. Tumino, S. Degl’Innocenti, P. P. Moroni, M. La Cognata, L. Pappalardo, and M. Sergi, *The Astrophysical Journal* **768**, 65 (2013).
 - [6] O. Fiedler and P. Kunze, *Nuclear Physics A* **96**, 513 (1967).
 - [7] C. Spitaleri, in *Exotic Nuclei And Nuclear/Particle Astrophysics* (World Scientific, 2006), pp. 316–323.
 - [8] F. Hammache, M. Heil, S. Typel, D. Galaviz, K. Sümmerer, A. Coc, F. Uhlig, F. Attallah, M. Caamano, D. Cortina, et al., *Physical Review C* **82**, 065803 (2010).
 - [9] A. Mukhamedzhanov, L. Blokhintsev, and B. Irgaziev, *Physical Review C* **83**, 055805 (2011).
 - [10] E. Tursunov, A. Kadyrov, S. Turakulov, and I. Bray, *Physical Review C* **94**, 015801 (2016).
 - [11] E. Tursunov, S. Turakulov, A. Kadyrov, and I. Bray, *Physical Review C* **98**, 055803 (2018).
 - [12] A. Mukhamedzhanov, R. Schmitt, R. E. Tribble, and A. Sattarov, *Physical Review C* **52**, 3483 (1995).
 - [13] F. Cecil, J. Yan, and C. S. Galovich, *Physical Review C* **53**, 1967 (1996).
 - [14] K. Langanke, *Nuclear Physics A* **457**, 351 (1986).
 - [15] K. Nollett, R. Wiringa, and R. Schiavilla, *Physical Review C* **63**, 024003 (2001).
 - [16] E. Tursunov, S. Turakulov, and P. Descouvemont, *Physics of Atomic Nuclei* **78**, 193 (2015).
 - [17] A. Kharbach and P. Descouvemont, *Physical Review C* **58**, 1066 (1998).
 - [18] R. G. Robertson, P. Dyer, R. Warner, R. Melin, T. Bowles, A. McDonald, G. Ball, W. Davies, and E. Earle, *Phys. Rev. Lett.:(United States)* **47** (1981).
 - [19] M. Anders, D. Trezzi, R. Menegazzo, M. Aliotta, A. Bellini, D. Bemmerer, C. Broggini, A. Caciolli, P. Corvisiero, H. Costantini, et al., *Physical Review Letters* **113**, 042501 (2014).
 - [20] P. Mohr, V. Kölle, S. Wilmes, U. Atzrott, G. Staudt, J. Hammer, H. Krauss, and H. Ober-

- hammer, Physical Review C **50**, 1543 (1994).
- [21] J. Kiener, H. Gils, H. Rebel, S. Zagromski, G. Gsottschneider, N. Heide, H. Jelitto, J. Wentz, and G. Baur, Physical Review C **44**, 2195 (1991).
 - [22] S. Igamov and R. Yarmukhamedov (1999).
 - [23] S. Typel, G. Bläge, and K. Langanke, Zeitschrift für Physik A Hadrons and Nuclei **339**, 335 (1991).
 - [24] N. Burkova, K. Zhaksibekova, M. Zhusupov, and R. Eramzhyan, Physics Letters B **248**, 15 (1990).
 - [25] G. Ryzhikh, R. Eramzhyan, and S. Shlomo, Physical Review C **51**, 3240 (1995).
 - [26] H. Hammer, C. Ji, and D. Phillips, Journal of Physics G: Nuclear and Particle Physics **44**, 103002 (2017).
 - [27] E. Ryberg, *Cluster effective field theory* (Chalmers Tekniska Hogskola (Sweden), 2016).
 - [28] K. Siegbahn, *Alpha-, beta-and gamma-ray spectroscopy* (Elsevier, 2012).
 - [29] F. Nazari, M. Radin, and M. M. Arani, The European Physical Journal A **59**, 20 (2023).
 - [30] R. Higa, G. Rupak, and A. Vaghani, The European Physical Journal A **54**, 1 (2018).
 - [31] J. Braun, W. Elkamhawy, R. Roth, and H. Hammer, Journal of Physics G: Nuclear and Particle Physics **46**, 115101 (2019).
 - [32] M. L. Goldberger and K. M. Watson, INC. New York-London-Sydney (1964).
 - [33] X. Kong and F. Ravndal, Nuclear Physics A **665**, 137 (2000).
 - [34] B. R. Holstein, Physical Review D **60**, 114030 (1999).
 - [35] R. Higa, H.-W. Hammer, and U. van Kolck, Nuclear Physics A **809**, 171 (2008).
 - [36] S.-I. Ando, The European Physical Journal A **52**, 130 (2016).
 - [37] H. Bethe, Physical Review **76**, 38 (1949).
 - [38] S.-i. Ando, J. W. Shin, C. H. Hyun, and S.-W. Hong, Physical Review C **76**, 064001 (2007).
 - [39] D. B. Kaplan, M. J. Savage, and M. B. Wise, Nuclear Physics B **534**, 329 (1998).
 - [40] M. Abramowitz and I. A. Stegun, *Handbook of mathematical functions* (1972).
 - [41] S.-I. Ando, The European Physical Journal A **57**, 17 (2021).
 - [42] S.-I. Ando, Physical Review C **100**, 015807 (2019).
 - [43] X. Kong and F. Ravndal, Physical Review C **64**, 044002 (2001).